

A Short History of (Orbital) Decay: Roman’s Prospects for Detecting Dying Planets

KYLEE CARDEN ¹, B. SCOTT GAUDI ¹ AND ROBERT F. WILSON ^{2,3}

¹*Department of Astronomy, The Ohio State University, 140 West 18th Ave., Columbus, OH 43210 USA*

²*Department of Astronomy, University of Maryland, College Park, MD, USA*

³*NASA Goddard Space Flight Center, 8800 Greenbelt Rd, Greenbelt, MD, USA*

ABSTRACT

The Roman Space Telescope Galactic Bulge Time Domain Survey (GBTDS) is expected to detect $\sim 10^5$ transiting planets. Many of these planets will have short orbital periods and are thus susceptible to tidal decay. We use a catalog of simulated transiting planet detections to predict the yield of orbital decay detections in the Roman GBTDS. Assuming a constant stellar tidal dissipation factor, Q'_* , of 10^6 , we predict $\sim 5 - 10$ detections. We additionally consider an empirical period-dependent parameterization of $Q'_* \propto P^{-3}$ and find a substantially suppressed yield. We conclude that Roman will provide constraints on the rate of planet engulfment in the Galaxy and probe the physics of tidal dissipation in stars.

Keywords: Exoplanets (498) — Exoplanet tides (497) — Surveys (1671) — Transits (1711)

1. INTRODUCTION

It has been known for some time that the excitation of tides by a satellite can result in orbital decay (Counselman 1973), which is thought to have played a role in the evolution of the Solar System (Goldreich & Soter 1966). Until the discovery of the first exoplanet around a Sun-like star (Mayor & Queloz 1995), there was only the Solar System and its one formation outcome to study. Since the first observation of an exoplanetary transit (Charbonneau et al. 2000), surveys have been conducted from the ground (e.g. Alonso et al. 2004; Bakos et al. 2004; Pollacco et al. 2006; Pepper et al. 2007) and space (e.g. Borucki et al. 2010; Howell et al. 2014; Ricker et al. 2015) to detect and characterize transiting planets. These surveys have detected thousands of short- and medium-period planets around hosts with a wide range of stellar properties.

Several studies (e.g. Maciejewski et al. 2018; Patra et al. 2020; Adams et al. 2024) have sought to detect exoplanet orbital decay, but there remain only two robust direct detections: WASP-12 b (Maciejewski et al. 2016; Patra et al. 2017) and Kepler-1658 b (Vissapragada et al. 2022). Indirect evidence suggests that decay sculpts the population of exoplanets we observe. Schlaufman &

Winn (2013) argue hot Jupiters are found less frequently around subgiant stars where tidal effects have shorter timescales, though the number of hot Jupiters around red giant stars complicates this picture (Grunblatt et al. 2019). Main sequence hot Jupiter host stars are younger than average, suggesting a hot Jupiter destruction mechanism (Hamer & Schlaufman 2019; Miyazaki & Masuda 2023). A recent detection of a transient associated with a planetary engulfment (De et al. 2023) further motivates searches for orbital decay.

The Nancy Grace Roman Space Telescope is NASA’s upcoming astrophysics flagship mission (Spergel et al. 2015). Roman will conduct the Galactic Bulge Time Domain Survey (GBTDS)¹ as one of its Core Community Surveys to detect cold and free-floating planets using microlensing (Bennett & Rhie 2002; Penny et al. 2019; Johnson et al. 2020) and complete a census of planets. The GBTDS will take advantage of Roman’s wide field-of-view and efficiency to observe $\sim 240 \times 10^6$ stars down to 25 mag in the broad (0.93 – 2.00-micron) F146 filter. High-precision observations towards the Galactic bulge over a long temporal baseline will produce science beyond microlensing, including the detection of an estimated $\sim 100,000$ warm and hot transiting planets

(Bennett & Rhie 2002; Montet et al. 2017; Wilson et al. 2023).

There is substantial historical precedence for the detection of transiting planets from microlensing surveys, including the first planet discovered by transits, OGLE-TR-56 b (Udalski et al. 2002). While radial velocities were used to confirm this planet (Konacki et al. 2003), this will generally not be possible with Roman given the faintness of most of the observed stars.

False positives are ubiquitous in transit surveys (Fressin et al. 2013), and robust vetting will be essential for Roman transiting exoplanet science. Various eclipsing binary (EB) configurations are especially nefarious astrophysical false positives (Cameron 2012), as they can mimic transit signals. Techniques employed by the Kepler and TESS surveys (e.g., centroid shifts, ellipsoidal variation, secondary eclipse detection, astrodensity profiling, Batalha et al. 2013; Sullivan et al. 2015; Kipping 2014) could be used for vetting candidates. Chromaticity checks using the transit depth inferred from observations in Roman’s secondary filter(s) could provide an additional means of validating short-period planet candidates.

Roman will expand transiting exoplanet science by 1) discovering planets in unexplored regions of the Galaxy, up to ~ 20 kpc away, that span the thin disk, thick disk, and bulge and 2) expanding the known transiting planet population by at least an order of magnitude (Wilson et al. 2023). This will enable demographic studies that probe the entire Galactic population of planets. The detection of an unprecedentedly large sample of planets will enable searches for intrinsically rare phenomena, such as orbital decay.

Perhaps the largest uncertainty in estimating a precise orbital decay yield comes from the stellar tidal dissipation factor Q_* , whose estimates can vary by orders of magnitude (e.g. Ogilvie & Lin 2007) from approximately $10^{5.5}$ to $> 10^8$ (Adams et al. 2024). The value of Q_* depends on the physical processes by which energy dissipates (Zahn 2008). Previous work has suggested Q_* depends on stellar mass, with the decay time only being short on the subgiant branch for the more massive stars (Weinberg et al. 2024), and on the tidal forcing frequency (i.e. the orbital period, see, e.g., Ogilvie & Lin 2007; Collier Cameron & Jardine 2018).

In this work, we consider the prospects for detecting orbital decay with the GBTDS. In Sec. 2, we lay out the features of the Roman Space Telescope, the Galactic Bulge Time Domain Survey, and a catalog of simulated transiting planet detections. In Sec. 3, we introduce formalism to estimate the signal of decay dP/dt in each simulated system and the accuracy with which Roman

can measure it. In Sec. 4, we use our formalism to address survey optimization and extensions and to estimate the yield of Roman orbital decay detections.

2. ROMAN AND THE GBTDS

The GBTDS will be carried out by the Wide Field Instrument (WFI) (Spergel et al. 2015). The technical specifications of the WFI are described in Akeson et al. (2019), and the most up-to-date values are listed on a NASA webpage.² The WFI will leverage Roman’s 2.4-m aperture primary mirror and 18 H4RG-10 4K x 4K detectors with broad near-infrared (NIR) sensitivity to achieve a field of view of 0.281 deg^2 , ~ 200 times larger than Hubble’s WFC3, while maintaining a similar resolution of $0.11''/\text{pixel}$ (Mosby et al. 2020). The WFI instrument includes eight overlapping filters spanning $0.48 - 2.3$ micron. The primary F146 survey filter spans $0.93 - 2.00$ micron with a PSF FWHM of 0.105 arcsec.

The Survey Definition Committee recently finalized its survey strategy recommendations³. These recommendations differ from the notional survey defined in Penny et al. (2019) in numerous ways, though most of these changes are of minimal consequence for orbital decay science. We proceed considering the notional survey, which has the following specifications:

1. six 72-day observing seasons centered on either the autumnal or vernal equinoxes when the Galactic bulge is visible from L2;
2. a survey baseline of 5 years with the observing seasons arranged as [1, 1, 1, 0, 0, 0, 0, 1, 1, 1], 1 = ON, 0 = OFF;
3. a 15-minute observing cadence (47 s exposures) for the primary filter F146 during each observing season; and
4. seven adjacent observing fields situated a couple of degrees from the Galactic Center

The Survey Definition Committee has laid out three distinct observing scenarios (underguide, nominal, and overguide). The number and placement of fields, season length, and cadence varies for each scenario. Since recent work advocated for changes to the season configuration (e.g. Gould 2024) and cadence (e.g. Kupfer et al. 2023), we focus on the ramifications of these two survey parameters for detecting orbital decay in Sec. 4.1. We

² https://roman.gsfc.nasa.gov/science/WFI_technical.html

³ https://asd.gsfc.nasa.gov/roman/comm_forum/forum.17/Core_Community_Survey_Reports-rev03-compressed.pdf

additionally consider the usefulness of extended observations for confirming decay candidates identified in the GBTDS.

Wilson et al. (2023) performed a pixel-level simulation of a single field of the Penny et al. (2019) notional survey to estimate a GBTDS yield of $\sim 60,000 - 200,000$ transiting planets. This simulation includes $\sim 59 \times 10^6$ stars with $F146 < 21$ as possible transiting planet hosts and led to a catalog of $\sim 9,000$ detected planets in one field. Wilson et al. (2023) followed the approach of Barclay et al. (2018) to simulate the exoplanet population, drawing the number of planets per star from a Poisson distribution consistent with estimated occurrence rates from Hsu et al. (2019) and then assigning each planet its properties and a host star. The planet occurrence rates were not scaled with metallicity, and thus the differences in the metallicities of the host stars in the inner thin disk, thick disk, and bulge, and the impact of metallicity on planet occurrence are neglected. As the occurrence rate of at least some types of planets increases with metallicity (e.g., Gonzalez 1997; Santos et al. 2001; Fischer & Valenti 2005; Buchhave et al. 2014), the yield may be underestimated.

3. METHODS

3.1. Transit Time Modeling

In order to detect orbital decay, a quadratic ephemeris model with a shrinking period must be statistically preferred over the simpler linear ephemeris model. An approximate expression for period decay (Goldreich & Soter 1966; Adams et al. 2024) is

$$\frac{dP}{dt} = - \left(\frac{27\pi}{2} \right) \left(\frac{M_p}{M_*} \right) \left(\frac{a}{R_*} \right)^{-5} \left(Q'_* \right)^{-1}, \quad (1)$$

where M_p is the planet mass, M_* is the stellar mass, a is the orbital semi-major axis, R_* is the stellar radius, and Q'_* is the stellar tidal dissipation factor. The linear ephemeris model is

$$T(E) = T_{0,lin} + P_{lin} \times E, \quad (2)$$

where $T(E)$ is the transit midpoint time predicted at epoch E , $T_{0,lin}$ is the reference ephemeris for $E = 0$, and P is the orbital period. The quadratic ephemeris model is

$$T(E) = T_{0,quad} + P_{quad} \times E + \frac{1}{2} \frac{dP}{dE} \times E^2, \quad (3)$$

where $T_{0,quad}$ is the reference ephemeris, and dP/dE is the derivative of the period P_{quad} .

With the catalog of simulated detected planets from Wilson et al. (2023) and an assumption about the stellar

tidal dissipation factor Q'_* , we can estimate the rate of orbital decay experienced by each system. We then need to estimate how well Roman will be able to constrain dP/dt .

3.2. Transit Time Covariance Matrix

To estimate the uncertainty with which we can constrain dP/dt , we follow the formalism laid out in Gould (2003) and Gould (2024). To make the analytic derivation simpler, we imagine observing one transit epoch at the central time of each season. Since the length of seasons (72 days) is small compared to the survey baseline (4.7 years), this simplification introduces only a small error, as we discuss in Sec. 3.4. We discuss an alternative season configuration in Sec. 4.1. Considering each season as a single observation translates to observing epochs

$$E_k = \left[-9, -7, -5, +5, +7, +9 \right] \frac{L}{P}, \quad (4)$$

where $L \equiv \text{yr}/4$ is half the minimum length of time between two observing season centers, P is the orbital period, and the epoch $E = 0$ is placed at the middle of the survey baseline.

We fit the observed transit times with a polynomial

$$F(E; a_i, \dots, a_r) = \sum_{i=0}^r a_i f_i(E), \quad (5)$$

where the trial functions $f_i(E), \dots, f_r(E)$ are terms from the truncated Taylor series, $f_i(E) = E^i/i!$, where $r = 1$ for the linear fit and $r = 2$ for the quadratic fit. In the quadratic case, we are fitting for coefficients a_i , where $a_0 = T_{0,quad}$, $a_1 = P_{quad}$, and $a_2 = dP/dE$ from Eq. 3. The entries of the inverse covariance matrix of the fit are then

$$b_{ij} = \sum_{k=1}^N \frac{1}{\sigma_0^2} \frac{\partial F}{\partial a_i} \frac{\partial F}{\partial a_j} = \sum_{k=1}^N \frac{f_i(E_k) f_j(E_k)}{\sigma_0^2} \quad (6)$$

with uncorrelated and constant uncertainties σ_0 in transit time measurements for each of the $N = 6$ seasons of observing.

Because the defined epochs in Eq. 4 are distributed symmetrically about $E = 0$, any matrix element b_{ij} where $i + j$ is odd is exactly 0. This leads to an inverse covariance matrix of

$$b \equiv c^{-1} = \frac{N}{\sigma_0^2} \begin{bmatrix} 1 & 0 & \langle E^2 \rangle / 2 \\ 0 & \langle E^2 \rangle & 0 \\ \langle E^2 \rangle / 2 & 0 & \langle E^4 \rangle / 4 \end{bmatrix}, \quad (7)$$

where

$$\langle E^t \rangle \equiv \frac{1}{N} \sum_k E_k^t. \quad (8)$$

This can be inverted to obtain the covariance matrix of

$$c = \frac{\sigma_0^2}{N} \begin{bmatrix} \frac{\langle E^4 \rangle}{\langle E^4 \rangle - \langle E^2 \rangle^2} & 0 & \frac{2\langle E^2 \rangle}{\langle E^2 \rangle^2 - \langle E^4 \rangle} \\ 0 & \frac{1}{\langle E^2 \rangle} & 0 \\ \frac{2\langle E^2 \rangle}{\langle E^2 \rangle^2 - \langle E^4 \rangle} & 0 & \frac{4}{\langle E^4 \rangle - \langle E^2 \rangle^2} \end{bmatrix}. \quad (9)$$

3.3. Analytic Uncertainty

Following the definition in Eq. 8, we find that the epoch averages are

$$\left\langle \left(\frac{P}{L} \right)^2 \right\rangle = \frac{155}{3} \text{ and } \left\langle \left(\frac{P}{L} \right)^4 \right\rangle = \frac{9587}{3}. \quad (10)$$

The uncertainty in T_0 is

$$\sigma_{T_0} = \sqrt{c_{00}} = \frac{\sqrt{9587}}{16\sqrt{37}} \sigma_0 \simeq 1.01 \sigma_0. \quad (11)$$

The uncertainty in P is

$$\sigma_P = \sqrt{c_{11}} = \frac{1}{\sqrt{310}} \frac{P}{L} \sigma_0 \simeq 0.057 \frac{P}{L} \sigma_0. \quad (12)$$

The uncertainty in dP/dE is

$$\sigma_{dP/dE} = \sqrt{c_{22}} = \frac{\sqrt{3}}{8\sqrt{37}} \frac{P^2}{L^2} \sigma_0 \simeq 0.036 \frac{P^2}{L^2} \sigma_0. \quad (13)$$

The period derivative $dP/dt = P^{-1} dP/dE$ depends on both P and dP/dE , and the uncertainty in dP/dt has contributions from both terms. However, the ratio of relative uncertainties is

$$\left(\frac{\sigma_{dP/dE}}{dP/dE} \right) \times \left(\frac{\sigma_P}{P} \right)^{-1} \simeq 0.6 \frac{P}{L dP/dt}. \quad (14)$$

Since the orbital period changes we are searching for are very small (i.e. $L dP/dt \ll P$), only the uncertainty in dP/dE contributes appreciably to uncertainty in dP/dt . This leads us to the expression

$$\sigma_{dP/dt} \approx \frac{\sqrt{3}}{8\sqrt{37}} \frac{P}{L^2} \sigma_0. \quad (15)$$

We adopt the analytic transit time uncertainty of

$$\sigma_{t_c} = Q^{-1} T \sqrt{\theta/2} \quad (16)$$

from Carter et al. (2008), where

$$Q \equiv \frac{\delta}{\sigma_{phot}} \sqrt{\Gamma T} \quad (17)$$

is the total signal-to-noise ratio of the transit in the limit $r \rightarrow 0$, $\theta \equiv \tau/T$ is the ratio of ingress/egress time to the total transit time T , Γ is the sampling rate or

inverse cadence, and σ_{phot} is photometric uncertainty per exposure. To first order, $\theta \sim \sqrt{\delta}$ so

$$\sigma_{t_c} \approx \sigma_{phot} \sqrt{\frac{T}{2\delta^{3/2}\Gamma}}, \quad (18)$$

The transit timing uncertainty for a season from Eq. 6 is $\sigma_0 = \sigma_{t_c}/\sqrt{n_s}$, where n_s is the number of transits observed per season, leading to an uncertainty in the period derivative of

$$\sigma_{dP/dt} \approx \frac{3}{8\sqrt{37}} \frac{P}{L^2} \sqrt{\frac{T}{\Gamma\delta^{3/2}}} \frac{\sigma_{phot}}{\sqrt{n_{tot}}}, \quad (19)$$

where $n_{tot} = 6n_s$ is the total number of transits observed over the duration of the survey.

3.4. Validation

Assuming that we observe only six transits at the middle of each season does introduce a small error in estimating the epoch averages. We are making the approximation that

$$\left\langle \left(\frac{P}{L} \right)^t \right\rangle \simeq \left(\frac{P}{L} \right)^t \frac{1}{M} \sum_{i=1}^M E_i^t, \quad (20)$$

where M is the full number of epochs that would actually be observed by Roman. Both of these approximations are good to less than 1% for periods < 5 days because the observing seasons are short compared to the survey baseline. This suggests we can estimate the uncertainty for each parameter accurately.

To check our analytic result, we simulate transits of planets of various periods with an injected decay signal, i.e., a period derivative. We keep only the transits that would be observed in GBTDS observing seasons. Then, we perform a quadratic fit, evaluate the uncertainty in T_0 , P , and dP/dE , all relative to σ_{t_c} , and find good agreement between the analytic estimates and the numerical results, as shown in Fig. 1.

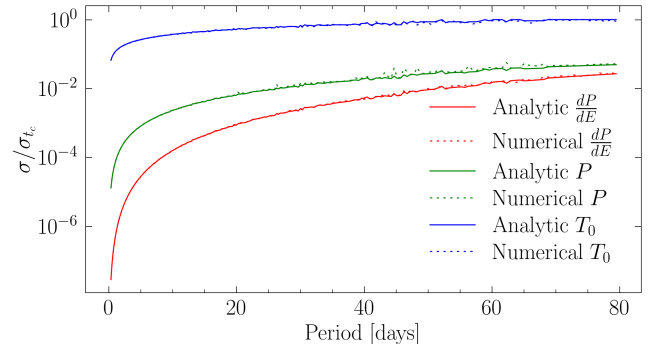


Figure 1. Comparison of the analytic estimate of uncertainty with the numerical results as a function of period, showing good agreement for all three parameters in the short-period regime.

4. ESTIMATING THE YIELD

4.1. Survey Optimization and Extensions

Although the GBTDS is essentially defined, we investigate the implications of survey parameters on orbital decay science. Gould (2024) suggested an alternative season configuration ([1, 1, 0, 0, 1, 1, 0, 0, 0, 1, 1], 1 = ON, 2 = OFF) better optimized for black hole science. This configuration translates to observing epochs

$$E_{k,G} = \left[-9, -7, -1, +1, +7, +9 \right] \frac{L}{P}. \quad (21)$$

Following the definition in Eq. 8, we find that

$$\left\langle \left(E \frac{P}{L} \right)^2 \right\rangle_G = \frac{131}{3} \text{ and } \left\langle \left(E \frac{P}{L} \right)^4 \right\rangle_G = \frac{8963}{3}. \quad (22)$$

Recalling Eq. 13, we can compare the uncertainty with which we can measure dP/dE

$$\frac{\sigma_{dP/dE}^G}{\sigma_{dP/dE}} = \sqrt{\frac{\langle E^4 \rangle - \langle E^2 \rangle^2}{\langle E^4 \rangle_G - \langle E^2 \rangle_G^2}} = \sqrt{\frac{37}{76}} \simeq 0.70, \quad (23)$$

using the values from Eq. 22. The Gould configuration leads to an uncertainty in dP/dt that is 70% of the uncertainty in the notional survey. Gould (2024) similarly found this improvement for measurements of astrometric accelerations with Roman.

The effects of other survey parameters are more subtle since they might also appreciably affect the number of transiting planets detected in addition to the uncertainty with which we can measure orbital decay. The cadences under consideration range from 12.1 to 14.8 min, suggesting a modest $\sim 10\%$ effect on measuring uncertainty in dP/dt due to differences in the number of data points. The Survey Definition Committee ultimately recommended 5 – 7 primary bulge fields plus a field at the Galactic Center. For large radii, high signal-to-noise ratio detections, this yield is approximately proportional to the number of sources, and thus going from 7 to 5 fields would decrease the yield by $\sim 30\%$. Assuming nothing about the properties of each field, each additional field simply increases the probability of finding a high-significance decay system because there are more systems in total.

Gould et al. (2024) advocated for doubling the sampling rate relative to the baseline Penny et al. (2019) survey design to $\Gamma = 8/\text{hr}$ (or one observation every 7.5 minutes), in order to increase the yield of low-mass free-floating planets detected by microlensing. This would require halving the number of fields, and would result in an increase in the yield of planets with small radii, but a decrease in the yield of planets with larger radii. If there

exists a large population of small, short period planets that are just below detectability with the nominal cadences of every 12.4 to 14.8 minutes, then this strategy could increase the yield of tidal decay detections dramatically. However, the Survey Definition Committee ultimately did not consider such high cadences. This may be an interesting strategy to consider in future campaigns during and extended Roman mission.

For survey extension to help, we must ensure the ephemerides remain accurate since we must know the epoch E corresponding to any transit. The number of orbits before the ephemeris is degraded is approximately

$$\frac{P}{\sigma_P} \approx \sqrt{\frac{155}{3}} L \frac{\sqrt{n_{tot}}}{\sigma_{t_c}} \quad (24)$$

For short-period planets orbiting bright stars, $n_{tot} > 100$ and $\sigma_{t_c} < 100$ min. This means that observations taken even years after the completion of the primary survey can be used to follow up decay candidates.

Since adding an additional season breaks the symmetry we used to construct the covariance matrix in Eq. 9, we numerically assessed the impact of adding an additional season. Season midpoints must be separated by at least six months given the bulge visibility windows. Fig. 2 shows the reduction in $\sigma_{dP/dt}$ that can be achieved with a single additional season whose midpoint is placed in a multiple of 6 months after the conclusion of the GBTDS. Additional observations after a few years have passed significantly improve our ability to measure dP/dt .

4.2. Catalog Detections

We analyzed the catalog of simulated planet detections from Wilson et al. (2023). It provides a planetary mass using the mass-radius relationship of Chen & Kipping (2017), stellar mass, planetary orbital period, stellar radius, planetary radius, transit duration,

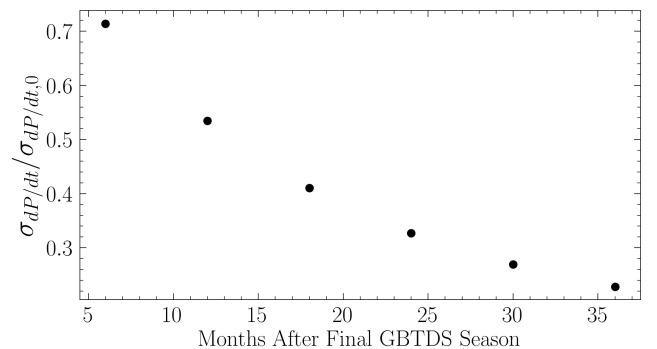


Figure 2. The reduction in uncertainty, relative to the GBTDS uncertainty $\sigma_{dP/dt,0}$, that can be achieved with an additional season of observing carried out some number of months after the conclusion of the GBTDS.

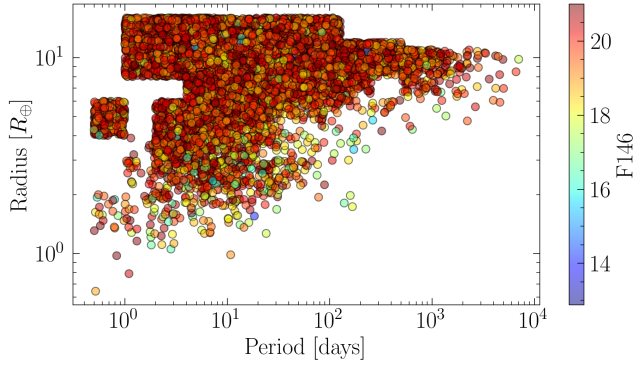


Figure 3. The distribution of the planets from the Wilson et al. (2023) simulated planet catalog in period and radius. The color bar indicates the apparent magnitude of each planet’s host star.

diluted transit depth, F146 magnitude, and number of transits observed for each simulated detection. It simulated a single field of transiting planet detections in the GBTDS. Fig. 3 shows the 9279 simulated detections in the space of period and radius. We find a few dozen planets within the Roche radii of their host stars and eliminate them from further analysis. We additionally assume eccentricity $e = 0$ in all cases. We use a noise model produced by The Roman IMage and TIME-series SIMulator⁴.

To estimate the yield of orbital decay detections, we need a model for the stellar tidal dissipation factor Q'_* , since there is little consensus on the mechanism or efficiency of tidal dissipation. There are several parametrizations of Q'_* that scale with the planet’s orbital period and occasionally other system properties

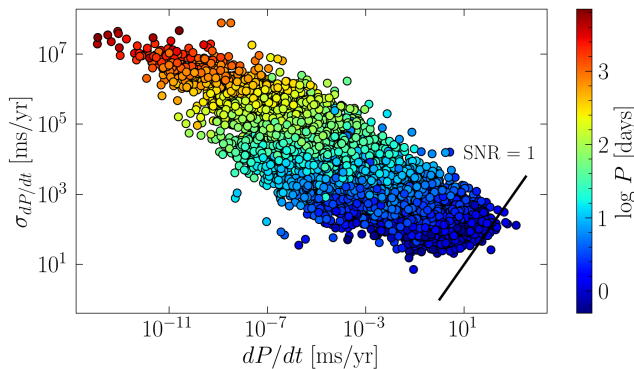


Figure 4. The distributions of dP/dt and $\sigma_{dP/dt}$ for each simulated planet detection. These quantities are highly correlated due to the strong dependence of each on the planet’s orbital period, as shown by the color bar. WASP-12 b has $dP/dt \sim 30$ ms/yr.

⁴ <https://github.com/robertfwilson/rimtimsim>

Table 1. High-Significance Systems

Quantity	#1923	#1399	#6041	#6286
M_* [M_\odot]	1.1	1.5	1.1	1.1
R_* [M_\odot]	2.7	2.3	3.0	2.5
F146	17.8	15.9	17.9	17.7
M_p [M_\oplus]	3930	1780	1430	4500
R_p [R_\oplus]	11.7	13.0	13.5	10.8
P [days]	1.00	1.03	1.07	1.23
dP/dt [ms/yr]	1290	122	576	478
$(dP/dt)/\sigma$	10	4.7	4.1	3.1

NOTE—Each simulated planet is identified with its index in the catalog.

(e.g. Essick & Weinberg 2016; Penev et al. 2018; Millholland et al. 2025). For our baseline estimate, we assumed a constant $Q'_* = 10^6$. Fig. 4 shows the resulting distributions of period derivatives dP/dt using Eq. 1 and their uncertainties using Eq. 19.

We then calculated the orbital decay signal-to-noise ratio, $\text{SNR} = (dP/dt)/(\sigma_{dP/dt})$ for each planet in the catalog. The system properties of the four highest SNR examples are reported in Table 1. They are massive planets orbiting bright stars with period derivatives generally much larger than those inferred for WASP-12 b and Kepler-1658 b.

To show what transit timing signal would look like with Roman, we simulated the detections of planet #1923 from Table 1 including the effect of decay from the dP/dt we estimated. We added Gaussian noise for the transit times and subtracted the best-fit linear model. The quadratic residuals that signal the decay of the orbit are shown in Fig. 5.

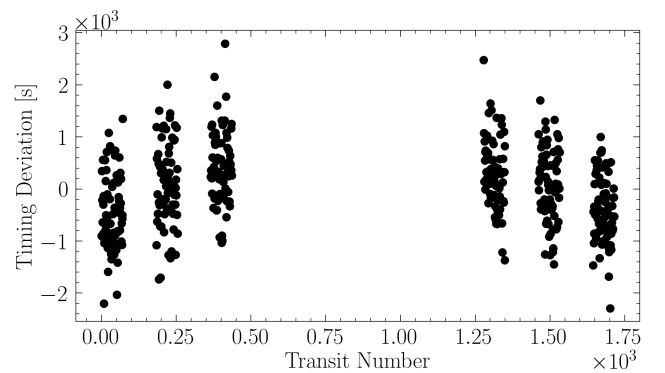


Figure 5. Example transit timing for planet #1923 in Table 1 from the GBTDS using the Penny et al. (2019) notional survey. This planet has the most robust detection of orbital decay in the simulated catalog.

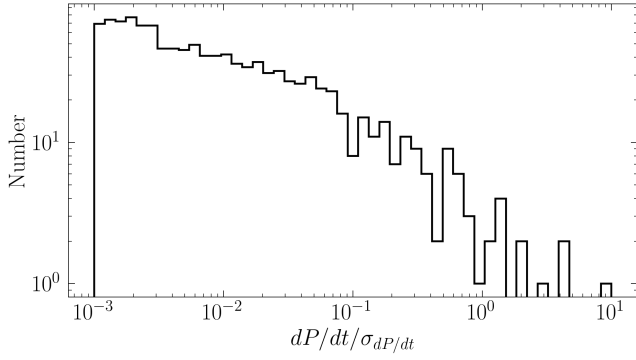


Figure 6. The histogram of orbital decay SNRs $> 10^{-3}$ using $Q'_* = 10^6$.

Fig. 6 shows the distribution of the orbital decay signal-to-noise ratios $> 10^{-3}$ for planets in the catalog using our baseline estimate assuming $Q'_* = 10^6$. Since Roman will find $\sim 100,000$ transiting planets, we must set a SNR threshold such that it is unlikely random fluctuations produce statistical false positives. $\text{SNR} = (dP/dt)/\sigma \simeq \sqrt{\Delta\chi^2}$, where $\Delta\chi^2$ compares the goodness-of-fit of the linear and quadratic models. $\Delta\chi^2$ follows a χ^2 distribution with one degree of freedom assuming uncorrelated, Gaussian noise. $P(\Delta\chi^2 > 19.5) \simeq 10^{-5}$, suggesting $\text{SNR} \simeq \sqrt{19.5} \simeq 4.4$ is a reasonable threshold for detection. We thus expect that 1 – 2 instances of orbital decay would be detectable for this catalog.

The actual number of bulge fields in the survey will be 5 – 7. Since the catalog only simulates the yield for one field, we expect the total yield to be $\sim 5\times$ larger, so we expect $\sim 5 - 10$ detections across the entire survey.

4.3. Alternative Parameterization

The exact form of Q'_* is not well-constrained. Millholland et al. (2025) argued using the known population of short period planets that

$$Q'_* = Q_0(P/2 \text{ days})^\alpha, \quad (25)$$

with $-4.33 \lesssim \alpha \lesssim -2$ and $10^{5.5} \lesssim Q_0 \lesssim 10^7$, suggesting less efficient tidal dissipation at short periods, consistent with Zanazzi et al. (2024). We adopted $\alpha = -3$ and $Q_0 = 10^6$ and then re-estimate the SNR distribution, as shown in Fig. 7. This form of Q'_* greatly reduces the decay rates for short periods to leave no detectable systems.

4.4. Caveats

Planet occurrence rates and properties in the Roman field might differ greatly from what we observe in the Solar neighborhood. The yield of orbital decay is likely

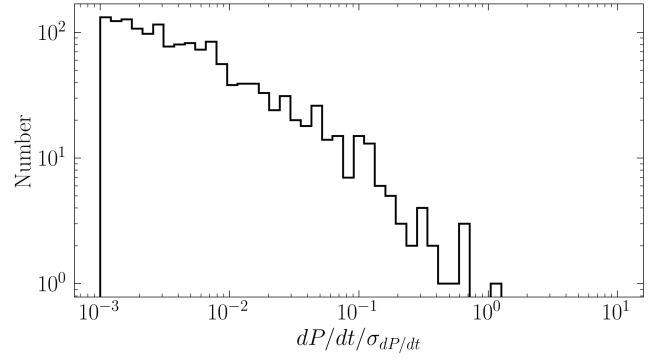


Figure 7. The histogram of orbital decay SNRs $> 10^{-3}$ using the Q'_* parameterization from Millholland et al. (2025).

to be especially sensitive to how many transiting planets Roman observes orbiting subgiant stars. Roman will set lower limits on Q'_* for an unprecedentedly large sample of transiting planet hosts, improving empirical constraints on Q'_* .

For a variety of factors, our yield estimate is likely overly conservative. First, the Wilson et al. (2023) catalog used occurrence rates with only upper limits for much of the parameter space where $P \lesssim 1$ day. We expect that the catalog underestimates the number of planets that will be detected in the regime of interest for orbital decay. Additionally, the catalog does not simulate planets around giants, which Roman is expected to detect.

Orbital decay is not the only phenomenon that causes deviations from a linear ephemeris model. Precession, dynamical perturbations from other bodies, and acceleration of the system along our line of sight can lead to a non-zero period derivative. Since dynamical interactions with other planets would be periodic, line-of-sight acceleration and apsidal precession are the most nefarious false positive scenarios. It often requires some detective work to decipher the physical origin of such a signal (e.g., Bouma et al. 2020; Ivshina & Winn 2022). Radial velocity measurements will be difficult to acquire for Roman stars so excluding line-of-sight acceleration might be difficult. One can exclude apsidal precession by timing secondary eclipses (Yee et al. 2020) or by inferring precession would require unphysically large planet Love numbers (Vissapragada et al. 2022). The latter of these approaches is likely to be more feasible with Roman stars.

5. CONCLUSIONS

We expect that Roman will be a powerful laboratory for probing orbital decay, a key mechanism for sculpting planetary demographics in the small-period regime. We expect 5 – 10 examples of orbital decay to be detectable

over the entire duration of the GBTDS. If these detections do come to fruition, they would expand the number of firm orbital decay detections by a factor of 2 or more.

Developing a pipeline for transit time fitting and deviations from a linear ephemeris will be crucial to actually identifying feasible decay candidates. Robust vetting of planet candidates and decay candidates will be essential to eliminate sources of false positives. Regardless of the actual yield, Roman transiting planets will provide a large, homogeneous sample with which to constrain the stellar tidal dissipation factor Q'_* of planet host stars.

6. ACKNOWLEDGMENTS

K.C. would like to thank Luke Bouma, Sarah Millholland, and Christopher Kochanek for useful comments and feedback. K.C., B.S.G., and R.F.W. were supported by NASA Grant 80NSSC24K0917. B.S.G. was additionally supported by the Thomas Jefferson Chair Endowment for Discovery and Space Exploration, and K.C. was additionally supported by the Ohio State Distinguished University Fellowship. The material is based upon work supported by NASA under award number 80GSFC24M0006.

Software: astropy (Collaboration et al. 2022), numpy (Harris et al. 2020), pandas (McKinney 2010), matplotlib (Hunter 2007)

REFERENCES

- Adams, E. R., Jackson, B., Sicafoose, A. A., et al. 2024, *The Planetary Science Journal*, 5, 163, doi: [10.3847/PSJ/ad3e80](https://doi.org/10.3847/PSJ/ad3e80)
- Akeson, R., Armus, L., Bachelet, E., et al. 2019, *The Wide Field Infrared Survey Telescope: 100 Hubbles for the 2020s*, doi: [10.48550/arXiv.1902.05569](https://doi.org/10.48550/arXiv.1902.05569)
- Alonso, R., Brown, T. M., Torres, G., et al. 2004, *ApJL*, 613, L153, doi: [10.1086/425256](https://doi.org/10.1086/425256)
- Bakos, G., Noyes, R. W., Kovács, G., et al. 2004, *Publications of the Astronomical Society of the Pacific*, 116, 266, doi: [10.1086/382735](https://doi.org/10.1086/382735)
- Barclay, T., Pepper, J., & Quintana, E. V. 2018, *The Astrophysical Journal Supplement Series*, 239, 2, doi: [10.3847/1538-4365/aae3e9](https://doi.org/10.3847/1538-4365/aae3e9)
- Batalha, N. M., Rowe, J. F., Bryson, S. T., et al. 2013, *The Astrophysical Journal Supplement Series*, 204, 24, doi: [10.1088/0067-0049/204/2/24](https://doi.org/10.1088/0067-0049/204/2/24)
- Bennett, D. P., & Rhie, S. H. 2002, *The Astrophysical Journal*, 574, 985, doi: [10.1086/340977](https://doi.org/10.1086/340977)
- Borucki, W. J., Koch, D., Basri, G., et al. 2010, *Science*, 327, 977, doi: [10.1126/science.1185402](https://doi.org/10.1126/science.1185402)
- Bouma, L. G., Winn, J. N., Howard, A. W., et al. 2020, *The Astrophysical Journal*, 893, L29, doi: [10.3847/2041-8213/ab8563](https://doi.org/10.3847/2041-8213/ab8563)
- Buchhave, L. A., Bizzarro, M., Latham, D. W., et al. 2014, *Nature*, 509, 593, doi: [10.1038/nature13254](https://doi.org/10.1038/nature13254)
- Cameron, A. C. 2012, *Nature*, 492, 48, doi: [10.1038/492048a](https://doi.org/10.1038/492048a)
- Carter, J. A., Yee, J. C., Eastman, J., Gaudi, B. S., & Winn, J. N. 2008, *The Astrophysical Journal*, Volume 689, Issue 1, pp. 499-512 (2008), 689, 499, doi: [10.1086/592321](https://doi.org/10.1086/592321)
- Charbonneau, D., Brown, T. M., Latham, D. W., & Mayor, M. 2000, *The Astrophysical Journal*, 529, L45, doi: [10.1086/312457](https://doi.org/10.1086/312457)
- Chen, J., & Kipping, D. 2017, *The Astrophysical Journal*, 834, 17, doi: [10.3847/1538-4357/834/1/17](https://doi.org/10.3847/1538-4357/834/1/17)
- Collaboration, A., Price-Whelan, A. M., Lim, P. L., et al. 2022, *The Astrophysical Journal*, 935, 167, doi: [10.3847/1538-4357/ac7c74](https://doi.org/10.3847/1538-4357/ac7c74)
- Collier Cameron, A., & Jardine, M. 2018, *Monthly Notices of the Royal Astronomical Society*, 476, 2542, doi: [10.1093/mnras/sty292](https://doi.org/10.1093/mnras/sty292)
- Counselman, III, C. C. 1973, *The Astrophysical Journal*, 180, 307, doi: [10.1086/151964](https://doi.org/10.1086/151964)
- De, K., MacLeod, M., Karambelkar, V., et al. 2023, *Nature*, 617, 55, doi: [10.1038/s41586-023-05842-x](https://doi.org/10.1038/s41586-023-05842-x)
- Essick, R., & Weinberg, N. N. 2016, *The Astrophysical Journal*, 816, 18, doi: [10.3847/0004-637X/816/1/18](https://doi.org/10.3847/0004-637X/816/1/18)
- Fischer, D. A., & Valenti, J. 2005, *ApJ*, 622, 1102, doi: [10.1086/428383](https://doi.org/10.1086/428383)
- Fressin, F., Torres, G., Charbonneau, D., et al. 2013, *The Astrophysical Journal*, 766, 81, doi: [10.1088/0004-637X/766/2/81](https://doi.org/10.1088/0004-637X/766/2/81)
- Goldreich, P., & Soter, S. 1966, *Icarus*, 5, 375, doi: [10.1016/0019-1035\(66\)90051-0](https://doi.org/10.1016/0019-1035(66)90051-0)
- Gonzalez, G. 1997, *MNRAS*, 285, 403, doi: [10.1093/mnras/285.2.403](https://doi.org/10.1093/mnras/285.2.403)
- Gould, A. 2003, arXiv e-prints, astro, doi: [10.48550/arXiv.astro-ph/0310577](https://doi.org/10.48550/arXiv.astro-ph/0310577)
- . 2024, *One Small Step for \$Roman\$; One Giant Leap for Black Holes*, doi: [10.48550/arXiv.2407.06484](https://doi.org/10.48550/arXiv.2407.06484)
- Gould, A., Yee, J. C., & Dong, S. 2024, arXiv e-prints, arXiv:2406.14531, doi: [10.48550/arXiv.2406.14531](https://doi.org/10.48550/arXiv.2406.14531)

- Grunblatt, S. K., Huber, D., Gaidos, E., et al. 2019, *The Astronomical Journal*, 158, 227, doi: [10.3847/1538-3881/ab4c35](https://doi.org/10.3847/1538-3881/ab4c35)
- Hamer, J. H., & Schlafman, K. C. 2019, *The Astronomical Journal*, 158, 190, doi: [10.3847/1538-3881/ab3c56](https://doi.org/10.3847/1538-3881/ab3c56)
- Harris, C. R., Millman, K. J., van der Walt, S. J., et al. 2020, *Nature*, 585, 357, doi: [10.1038/s41586-020-2649-2](https://doi.org/10.1038/s41586-020-2649-2)
- Howell, S. B., Sobek, C., Haas, M., et al. 2014, *Publications of the Astronomical Society of the Pacific*, 126, 398, doi: [10.1086/676406](https://doi.org/10.1086/676406)
- Hsu, D. C., Ford, E. B., Ragozzine, D., & Ashby, K. 2019, *AJ*, 158, 109, doi: [10.3847/1538-3881/ab31ab](https://doi.org/10.3847/1538-3881/ab31ab)
- Hunter, J. D. 2007, *Computing in Science & Engineering*, 9, 90, doi: [10.1109/MCSE.2007.55](https://doi.org/10.1109/MCSE.2007.55)
- Ivshina, E. S., & Winn, J. N. 2022, *The Astrophysical Journal Supplement Series*, 259, 62, doi: [10.3847/1538-4365/ac545b](https://doi.org/10.3847/1538-4365/ac545b)
- Johnson, S. A., Penny, M., Gaudi, B. S., et al. 2020, *The Astronomical Journal*, 160, 123, doi: [10.3847/1538-3881/aba75b](https://doi.org/10.3847/1538-3881/aba75b)
- Kipping, D. M. 2014, *Monthly Notices of the Royal Astronomical Society*, 440, 2164, doi: [10.1093/mnras/stu318](https://doi.org/10.1093/mnras/stu318)
- Konacki, M., Torres, G., Jha, S., & Sasselov, D. D. 2003, *Nature*, 421, 507, doi: [10.1038/nature01379](https://doi.org/10.1038/nature01379)
- Kupfer, T., Danielski, C., Gandhi, P., et al. 2023, *The continuous cadence Roman Galactic Bulge survey*, doi: [10.48550/arXiv.2306.14956](https://doi.org/10.48550/arXiv.2306.14956)
- Maciejewski, G., Dimitrov, D., Fernández, M., et al. 2016, *Astronomy and Astrophysics*, 588, L6, doi: [10.1051/0004-6361/201628312](https://doi.org/10.1051/0004-6361/201628312)
- Maciejewski, G., Fernández, M., Aceituno, F., et al. 2018, *Acta Astronomica*, 68, 371, doi: [10.32023/0001-5237/68.4.4](https://doi.org/10.32023/0001-5237/68.4.4)
- Mayor, M., & Queloz, D. 1995, *Nature*, 378, 355, doi: [10.1038/378355a0](https://doi.org/10.1038/378355a0)
- McKinney, W. 2010, *scipy*, doi: [10.25080/Majora-92bf1922-00a](https://doi.org/10.25080/Majora-92bf1922-00a)
- Millholland, S. C., MacLeod, M., & Xiao, F. 2025, *ApJ*, 981, 77, doi: [10.3847/1538-4357/ada76d](https://doi.org/10.3847/1538-4357/ada76d)
- Miyazaki, S., & Masuda, K. 2023, *The Astronomical Journal*, 166, 209, doi: [10.3847/1538-3881/acff71](https://doi.org/10.3847/1538-3881/acff71)
- Montet, B. T., Yee, J. C., & Penny, M. T. 2017, *Publications of the Astronomical Society of the Pacific*, 129, 044401, doi: [10.1088/1538-3873/aa57fb](https://doi.org/10.1088/1538-3873/aa57fb)
- Mosby, G., Rauscher, B. J., Bennett, C., et al. 2020, *Journal of Astronomical Telescopes, Instruments, and Systems*, 6, 046001, doi: [10.1117/1.JATIS.6.4.046001](https://doi.org/10.1117/1.JATIS.6.4.046001)
- Ogilvie, G. I., & Lin, D. N. C. 2007, *The Astrophysical Journal*, 661, 1180, doi: [10.1086/515435](https://doi.org/10.1086/515435)
- Patra, K. C., Winn, J. N., Holman, M. J., et al. 2017, *The Astronomical Journal*, 154, 4, doi: [10.3847/1538-3881/aa6d75](https://doi.org/10.3847/1538-3881/aa6d75)
- . 2020, *The Astronomical Journal*, 159, 150, doi: [10.3847/1538-3881/ab7374](https://doi.org/10.3847/1538-3881/ab7374)
- Penev, K., Bouma, L. G., Winn, J. N., & Hartman, J. D. 2018, *The Astronomical Journal*, 155, 165, doi: [10.3847/1538-3881/aaaf71](https://doi.org/10.3847/1538-3881/aaaf71)
- Penny, M. T., Gaudi, B. S., Kerins, E., et al. 2019, *The Astrophysical Journal Supplement Series*, 241, 3, doi: [10.3847/1538-4365/aafb69](https://doi.org/10.3847/1538-4365/aafb69)
- Pepper, J., Pogge, R. W., DePoy, D. L., et al. 2007, *Publications of the Astronomical Society of the Pacific*, 119, 923, doi: [10.1086/521836](https://doi.org/10.1086/521836)
- Pollacco, D. L., Skillen, I., Collier Cameron, A., et al. 2006, *Publications of the Astronomical Society of the Pacific*, 118, 1407, doi: [10.1086/508556](https://doi.org/10.1086/508556)
- Ricker, G. R., Winn, J. N., Vanderspek, R., et al. 2015, *Journal of Astronomical Telescopes, Instruments, and Systems*, 1, 014003, doi: [10.1117/1.JATIS.1.1.014003](https://doi.org/10.1117/1.JATIS.1.1.014003)
- Santos, N. C., Israelian, G., & Mayor, M. 2001, *A&A*, 373, 1019, doi: [10.1051/0004-6361:20010648](https://doi.org/10.1051/0004-6361:20010648)
- Schlaufman, K. C., & Winn, J. N. 2013, *The Astrophysical Journal*, 772, 143, doi: [10.1088/0004-637X/772/2/143](https://doi.org/10.1088/0004-637X/772/2/143)
- Spergel, D., Gehrels, N., Baltay, C., et al. 2015, *Wide-Field Infrared Survey Telescope-Astrophysics Focused Telescope Assets WFIRST-AFTA 2015 Report*, doi: [10.48550/arXiv.1503.03757](https://doi.org/10.48550/arXiv.1503.03757)
- Sullivan, P. W., Winn, J. N., Berta-Thompson, Z. K., et al. 2015, *The Astrophysical Journal*, 809, 77, doi: [10.1088/0004-637X/809/1/77](https://doi.org/10.1088/0004-637X/809/1/77)
- Udalski, A., Zebrun, K., Szymanski, M., et al. 2002, *Acta Astronomica*, 52, 115, doi: [10.48550/arXiv.astro-ph/0207133](https://doi.org/10.48550/arXiv.astro-ph/0207133)
- Vissapragada, S., Chontos, A., Greklek-McKeon, M., et al. 2022, *The Astrophysical Journal*, 941, L31, doi: [10.3847/2041-8213/aca47e](https://doi.org/10.3847/2041-8213/aca47e)
- Weinberg, N. N., Davachi, N., Essick, R., et al. 2024, *The Astrophysical Journal*, 960, 50, doi: [10.3847/1538-4357/ad05c9](https://doi.org/10.3847/1538-4357/ad05c9)
- Wilson, R. F., Barclay, T., Powell, B. P., et al. 2023, *The Astrophysical Journal Supplement Series*, 269, 5, doi: [10.3847/1538-4365/acf3df](https://doi.org/10.3847/1538-4365/acf3df)
- Yee, S. W., Winn, J. N., Knutson, H. A., et al. 2020, *The Astrophysical Journal*, 888, L5, doi: [10.3847/2041-8213/ab5c16](https://doi.org/10.3847/2041-8213/ab5c16)
- Zahn, J. P. 2008, in *EAS Publications Series*, Vol. 29, *EAS Publications Series*, ed. M. J. Goupil & J. P. Zahn, 67–90, doi: [10.1051/eas:0829002](https://doi.org/10.1051/eas:0829002)

Zanazzi, J. J., Dewberry, J., & Chiang, E. 2024, *The Astrophysical Journal*, 967, L29,
doi: [10.3847/2041-8213/ad4644](https://doi.org/10.3847/2041-8213/ad4644)